# Four-Fold Color Filter Based on Plasmonic Phase Retarder

Luc Duempelmann,[†,‡] Angélique Luu-Dinh,[†] Benjamin Gallinet,*[,†] and Lukas Novotny[‡]

[†]CSEM, Thin Film Optics, Muttenz, 4132, Switzerland

[‡]ETHZ Zürich, D-ITET, Zürich, 8092, Switzerland

ⓢ Supporting Information

ABSTRACT: We present a plasmonic color filter based on periodic subwavelength silver nanowires, capable of changing the output color by simple rotation of a polarizer. The effect is enabled by a wavelength-dependent phase shift near the plasmon resonance, giving rise to a wavelength-dependent rotation of the incident polarization. Subsequent rotation of an analyzing polarizer leads to an output of four distinct colors (e.g., yellow, blue, purple, and red) and combinations thereof. The plasmon resonance itself can be tuned throughout the visible spectral region by proper choice of fabrication parameters.
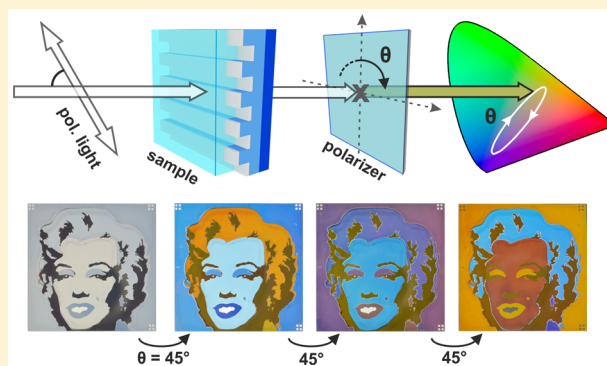
KEYWORDS: tunable color filter, plasmonic polarizer, localized surface plasmon resonance, structural colors, phase retarder, silver

Plasmonic structures have been of great interest in the last decades as use for structural colors,[1] optical filters, and metasurfaces for wavefront control. Besides ease of fabrication, wide tune-ability, and stability of the colors, they outperform the chemical counterparts thanks to their high resolution beyond the diffraction limit and higher compactness.[2,3] Recently, plasmonic transmission filters tunable over the whole visible range have been demonstrated.[4−9] This makes them well suited for display technologies or imaging applications,[10] where in particular the control of polarization is essential. Devices controlling the polarization state, for example, wave retarders, are realized by using birefringent materials (e.g., mica),[11] liquid crystals, or more recently, diffraction gratings.[12] Phase retardation is caused by different propagation speeds along the crystal axes and requires a certain thickness of the crystal. In contrast, wave retarders based on thin plasmonic or metasurface substrates can induce a phase shift at the resonance of the structure or the surface itself, leading to a control of the output polarization.[13−17] This principle has recently also been utilized for metasurface holograms.[15,18] The origin of this polarization control is that the excitation of localized surface plasmon resonances (LSPR) depends intrinsically on the polarization of the incident light.[19] This polarization sensitivity was exploited for stereo view in reflection[20] and spectrally tunable transmission filters.[4] Switching between states is enabled by changing the polarization of the incident light with a passive polarizer or an integrated tunable layer (such as an electrically tunable liquid crystal).[21]

Novel display technologies and CMOS sensors show a great need for compact optical filters capable of actively changing the output color[4,9,21−23] or polarization[24] and being able to act as photodetectors.[10] Existing filters are often bulky, limited in the acting region, or costly and not integratable in high-throughput fabrication processes. Transmissive filters based on plasmonics are interesting candidates due to their compactness and color tunability,[2,3,5,9,25,26] even on flexible substrates.[27] Until now they were often limited to a specific range of colors and suffer from fabrication complexity. On the other hand, plasmonic phase retarders show great potential in shaping the incident polarization,[28] but are often designed to be independent of wavelength (achromatic) or active only in the infrared or microwave range.[11,12]

Here we introduce a plasmonic phase retarder (PPR) that performs 4-fold color filtering in the visible spectral range. The substrate altering the polarization of the incident light consists of a periodic array of silver nanowires. This structure supports localized surface plasmon resonances (LSPR) capable of inducing a strong phase shift for one polarization setting. As a result, the rotation of an analyzing colorless polarizer gives rise to four distinct colors and their combinations. We optimize the geometry to make the optical effect independent of the tilt angle,[29,30] enabling use in ambient light conditions. Our structures have been fabricated with an upscalable and cost-effective process and are designed to be resistant to wear.

Subwavelength silver nanowires are fabricated by nanoimprint lithography and standard metal evaporation. The parameters of the nanostructures, such as the period and depth, were optimized to decrease the angle- and orientation-dependency of the generated color and to tune the localized surface plasmon resonance (LSPR) into the visible (see Figure S1). The thickness of the silver nanowires also influences the position of the LSPR and was chosen to be in the range of 10−30 nm. With lower

thickness the resonance disappears and with higher thickness the transmission decreases. After evaporation of silver the sample is embedded in UV-curable polymer providing protection for ambient use.

Figure 1a illustrates the working principle of the plasmonic phase retarder (PPR) consisting of periodically aligned subwavelength silver nanowires. Linearly polarized visible light is incident on the PPR perpendicular or parallel to the nanowires. We distinguish between p-pol (p-polarization) and s-pol (s-polarization), which are referred to as transverse-magnetic (TM) and transverse-electric (TE), respectively, in other literature. The corresponding measured transmission spectra are shown in Figure 1b. A localized surface plasmon resonance (LSPR) is excited in p-pol leading to a resonant dip (at λ_R) in the spectra. The spectrum of s-pol light is broadband with no sharp resonances. The spectrum of mixed-pol (superposition of p-pol and s-pol) is relatively flat and corresponds to the average of the p-pol and s-pol spectra. It renders the spectrum of unpolarized light but with slightly lower intensity.

To generate distinct colors we set the input polarizer to $\theta_1 = 45°$ (diagonally polarized) and add an additional polarizer with settings $\theta_2 = 0°, 45°, 90°$, and $135°$ to the output of the PPR. The resulting four transmission spectra are shown in Figure 1d. For $\theta_2 = 0°$ and $\theta_2 = 90°$, we obtain spectra similar to s-pol and p-pol in Figure 1a, respectively, but with an intensity decreased by $1/(2)^{1/2}$. In contrary, the spectra for $\theta_2 = 45°$ and $\theta_2 = 135°$ clearly differ from the transmission spectrum of the PPR with mixed input state (Figure 1b), which is an indication of birefringence (like liquid crystals). This wavelength-dependent birefringence leads to a rotation of the incident polarization, such that the transmission through the analyzing polarizer is enhanced or weakened as a function of the wavelength, depending on the polarization angle. Since a strong spectral change is observed near the plasmon resonance λ_R we conclude that the plasmonic resonance (excited by p-pol) is the main reason for the wavelength-dependent rotation of the phase. As illustrated in Figure 1c, a phase shift of p-pol causes the in-phase peak intensity (I_{max}) to change direction (see * below and † above the resonance, respectively), giving rise to four distinct spectra (see Figure 1d) and combinations thereof. The rapid phase change near the plasmon resonance can be described by a harmonic oscillator model: the sharper the resonance is, the faster the phase changes and the more rapid is the transition between the diagonal states ($\theta_2 = 45°$ and $135°$). Consequently, the contrast of these states is considerably stronger than the contrast of the pure s-pol and p-pol states. The color values used in Figure 1b,d have been extracted from measurements. We multiplied the lightness values (L) by 1.5 (in HSL color space) to increase visibility. This is linked to an increase of the illumination source.

Figure 2 shows measured transmission spectra for different settings of the input polarization ($\theta_1 = 0°, 45°, 90°$, and $135°$) and as a function of the output polarization angle ($0° < \theta_2 < 360°$, in steps of $1°$). For $\theta_1 = 0°$ and $90°$, the maxima of the p-pol state (at $\theta_2 = 0°$) and s-pol state (at $\theta_2 = 90°$) are clearly visible (Figure 1b). For both the s-pol and the p-pol states, the transmission is blocked if the analyzing polarizer is at a right angle to the incident polarization. Accordingly, if $\theta_1 = \theta_2$, the transmission is at a maximum, and if $\theta_1 = \theta_2 + 90°$, the transmission is
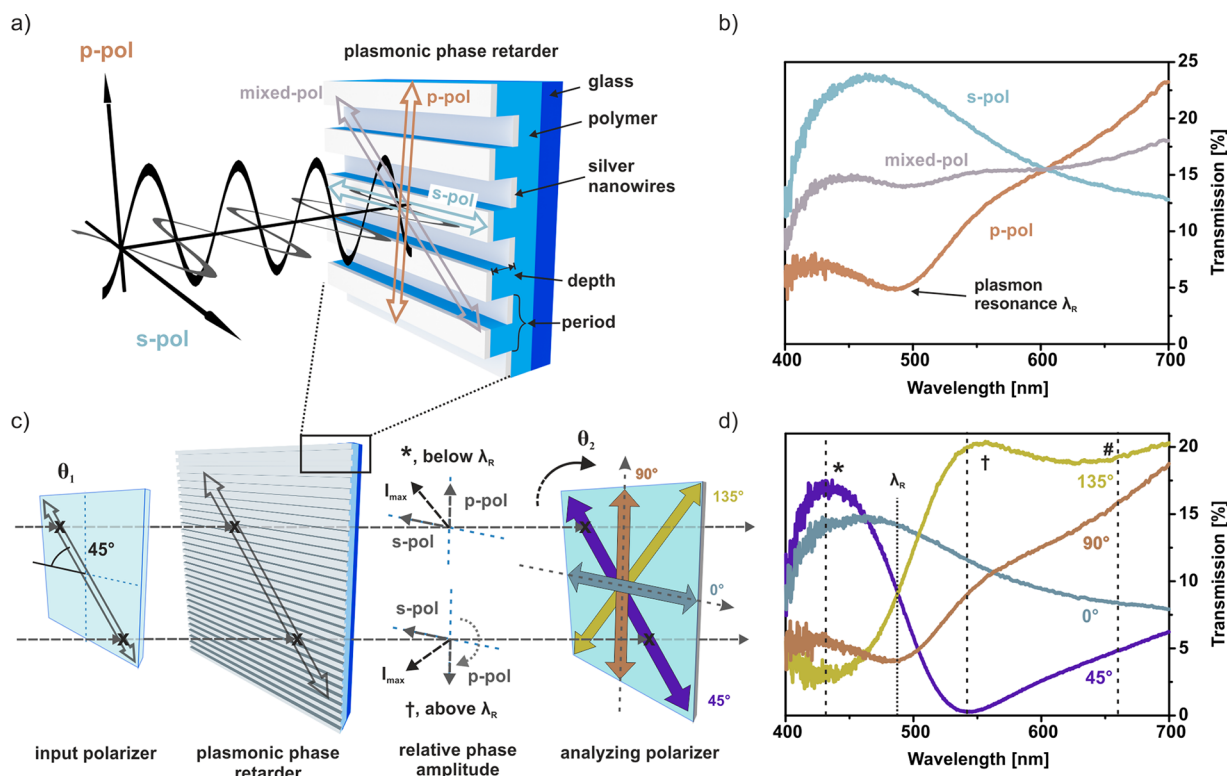
Figure 1. Basic principle of the plasmonic phase retarder (PPR) and its application as color filter. (a) Sketch of the PPR prior embedding, displaying the orientation of s-, p-, and mixed-polarized light. (b) Measured transmission spectra for s-pol, p-pol, and mixed-pol. (c) Color filter based on the PPR with diagonally polarized incident light ($\theta_1 = 45°$) and a variable analyzing polarizer. The transmission after the PPR can be described by the relative phase amplitudes of p-pol and s-pol (see sketch), where the phase shift of p-pol near the plasmon resonance λ_R leads to an angular change of the peak intensity (I_{max}). Distinct colors are generated after passing through the analyzing polarizer (d). The spectra and states are shown in terms of the measured colors.
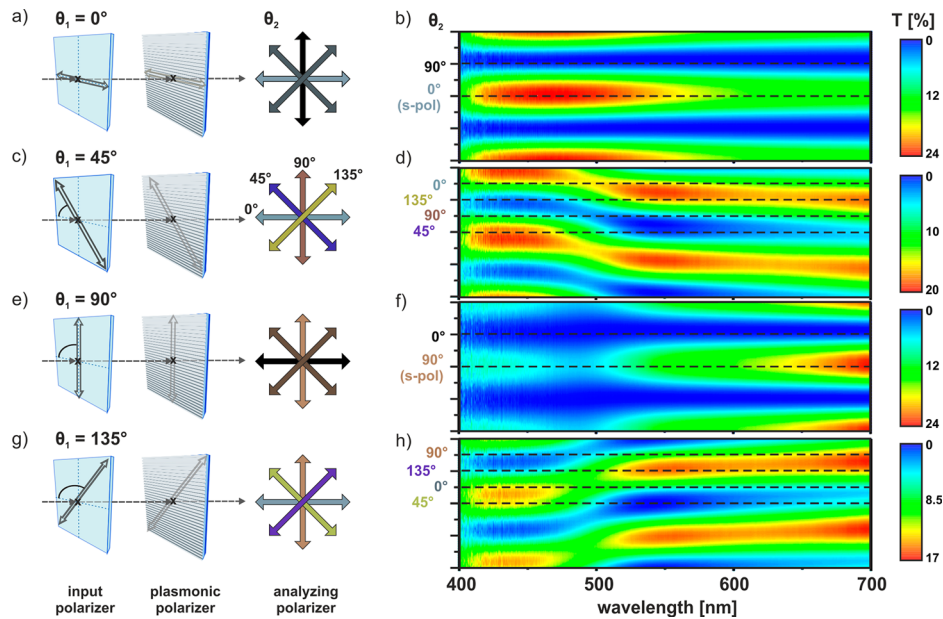
Figure 2. Transmission spectra as a function of polarization angles. (Left) Measurement schemes for different angles of the incident polarizer (θ_1) and the analyzing polarizer (θ_2), each output arrow is colored in the observed color (as in Figure 1d). (Right) Corresponding transmission plots for rotation of the analyzing polarizer ($0° < \theta_2 < 360°$, 1° steps).

zero (see Figure 2b,f). This trivial configuration can be described with two polarizers and a color filter in between. The situation is more intricate for diagonal input polarization ($\theta_1 = 45°$ and 135°). Here, s-pol and p-pol acquire a different phase shift that depends on the wavelength. The polarization state after the PPR is therefore elliptical and the orientation of the ellipse is a function of wavelength. Very different colors are therefore obtained for different settings of the analyzing polarizer (θ_2). Figure 2d,h shows that the transmission spectra sensitively depend on the setting of θ_2. The total intensities are conserved but the maxima shift as θ_2 is varied. This is a clear indication of a phase shift. Similar results were observed for other plasmonic resonant systems.[13] The phase shift is responsible for the observation of four distinct output colors in the diagonal case ($\theta_1 = 45°$ and 135°); only one color is observed for each s-pol and p-pol ($\theta_1 = 0°$ and 90°).

The transmission spectra shown in Figure 2 can be described with the knowledge of the polarization states and the phase information, which can be formulated in terms of Jones Matrices.[31] The field transmitted through input polarizer, PPR, and analyzing polarizer is

$$E(\theta_1, \theta_2) = \begin{bmatrix} \cos^2 \theta_2 & \sin \theta_2 \cos \theta_2 \\ \sin \theta_2 \cos \theta_2 & \sin^2 \theta_2 \end{bmatrix}_{\text{analyzing polarizer}} \begin{bmatrix} E_s e^{i\varphi_s} & 0 \\ 0 & E_p e^{i\varphi_p} \end{bmatrix}_{\text{PPR}} \begin{bmatrix} \cos \theta_1 \\ \sin \theta_1 \end{bmatrix}_{\text{input pol}} \quad (1)$$

E_s and E_p are the field amplitudes of the s-pol and p-pol states, respectively, and φ_s and φ_p are the corresponding phases. The square modulus $|E|^2$ is proportional to the transmitted intensity and becomes

$$|E(\theta_1, \theta_2)|^2 = \{(E_s \cos \theta_1 \cos \theta_2 \cos \varphi_s + E_p \sin \theta_1 \sin \theta_2 \cos \varphi_p)^2$$
$$+ (E_s \cos \theta_1 \cos \theta_2 \sin \varphi_s + E_p \sin \theta_1 \sin \theta_2 \sin \varphi_p)^2\} \quad (2)$$

This formula describes all the measured states in Figure 2 and requires only the intensity of the incident polarized light and the corresponding phase shift caused by the PPR. For $\theta_1 = 0°$ or 90°,

we obtain the two orthogonal states s-pol and p-pol, whereas for $\theta_1 = 45°$ or 135°, there are four different states due to the phases φ_s and φ_p.

To understand the origin of the phase variations we performed electromagnetic field calculations using the surface integral equation method (SIE).[32] This computational method provides high accuracy in the near-field and is especially advantageous for open boundary conditions. Figure 3a displays the simulated transmission spectra for s-pol and p-pol input states. The calculated spectra reproduce our measurements (Figure 1b), although the overall intensity is a factor of 3 lower in the
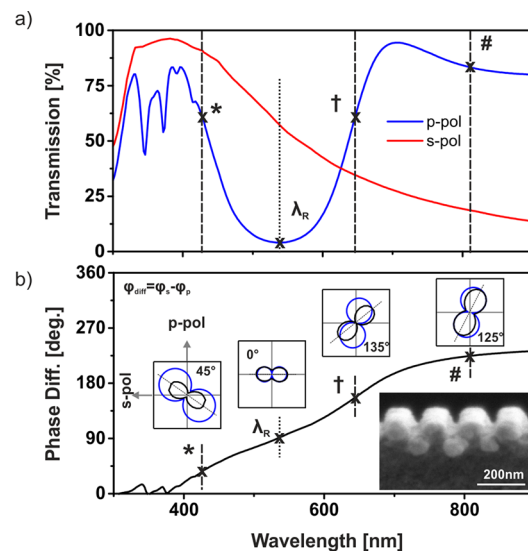

Figure 3. Theoretical analysis of the plasmonic color filter. (a) Calculated transmission spectra for s-pol and p-pol. (b) Corresponding phase difference between s-pol and p-pol. The insets indicate the angle-dependent intensity distribution of the output (as a function of θ_2, c.f., Figure 1c,d). The SEM image shows the fabricated structure prior embedding.

measurements. The optical properties of silver can strongly suffer from gas or water residues during the evaporation process.[33] Further, silver "is susceptible to dewetting and grain-boundary pinning".[33] Smooth surfaces can be achieved using high evaporation rates and high vacuum conditions. However, our vacuum is limited to 5×10^{-6} mbar, and our evaporation rates cannot be increased without sacrificing process control. Nevertheless, both parameters can be optimized in the future. For example, we observed a transmission increase of ∼15% when increasing the evaporation rates from 3 to 30 Å/s (data not shown). This increase only caused a small shift of the spectra and consequently the same color was observed. Therefore, the fabrication conditions are not critical for achieving the color effects described here; they mainly affect the overall transmission. It should be noted that absorption of the UV-curable polymer in the blue leads to a decrease of the transmission for wavelengths shorter than ∼430 nm, see Figure 1b,d.

With the help of SIE we can determine the device parameters, that is, the amplitudes E_s, E_p, and the phases φ_p and φ_s. These parameters can also be determined by fitting eq 2 to the measured transmission spectra (Figure 2). As shown in Figure 3b, the calculated phase difference $\varphi_{diff} = \varphi_p - \varphi_s$ shows a pronounced increase (∼180°) near the plasmon resonance. The insets in Figure 3b show the transmitted intensity as a function of the output angle θ_2 for wavelengths below (*), at (λ_R), above (†), and far above (#) the plasmon resonance. The blue curves are calculations and the black curves are measurements (intensity multiplied by 3). A slight deviation between theory and measurement is observed just above the resonance (†), which is caused by a slightly broader LSPR resonance in the simulations. The angles in the insets indicate the angles for which the measured transmitted intensity is highest. A more detailed investigation of the origin of the phase shift is given in Figure S2. The calculated electromagnetic near-field and the electric charge distribution both show a clear change around the plasmon resonance. Similar effects near LSPRs have been reported in the literature before.[14,34]

In a next step, we studied the influence of geometric parameters, such as the etching depth (vertical separation between nanowire layers) and the thickness of the nanowires. Figure 4a,b shows the corresponding simulated transmission plots for p-polarized light. These simulations were carried out using rigorous coupled-wave analysis (RCWA).[35] The lines in Figure 4a show the location of two modes, one being the LSPR (dashed) and a second (dot-dashed) that depends on the in-plane interaction between the nanowires. This second mode shifts to higher energy for decreasing depth, which is an indication for a quadruple mode. For depths larger than 90 nm, the two layers of nanowires are sufficiently separated, and their interaction can be neglected. Experimentally we have verified this effect with nanostructures having a depth of 70 and 90 nm (data not shown). Combining the effects of different silver nanowire thicknesses (see Figure 4b) with different nanostructure depths yields a wide range of distinct colors, spanning the complete visible range excited by s-pol and p-pol light (see Figure 4c).
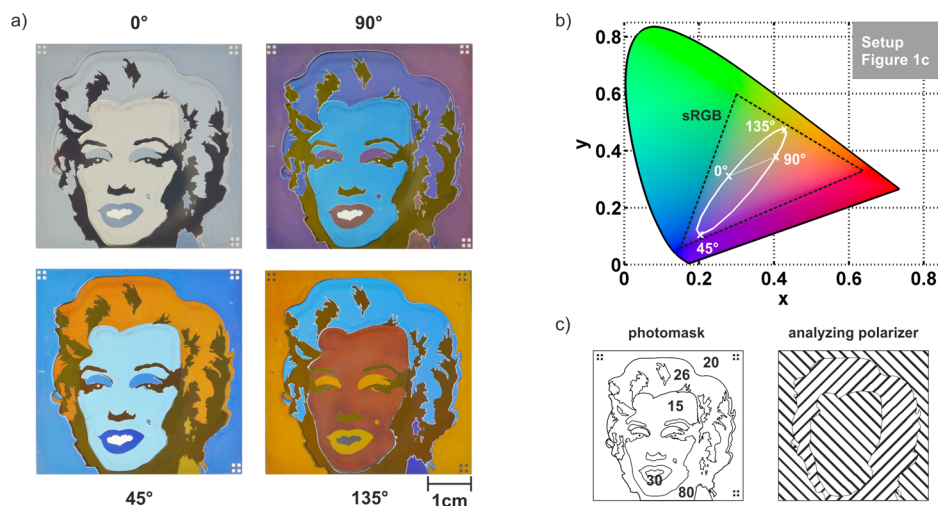
Figure 5a,b shows images of Marilyn Monroe ("Marilyn Diptych" by Andy Warhol, 1962) and an exemplary CIE xyY color plot (CIE 1931 color space).[36] This Marilyn Monroe image was one of the first commercial large-scale productions of art made by silkscreen. The images in Figure 5a were recorded with a diagonal input polarizer (c.f. Figure 1c) and different settings of the output polarizer. The CIE xyY color plot, displaying sample of Figure 1, shows four distinct states and intermediate colors
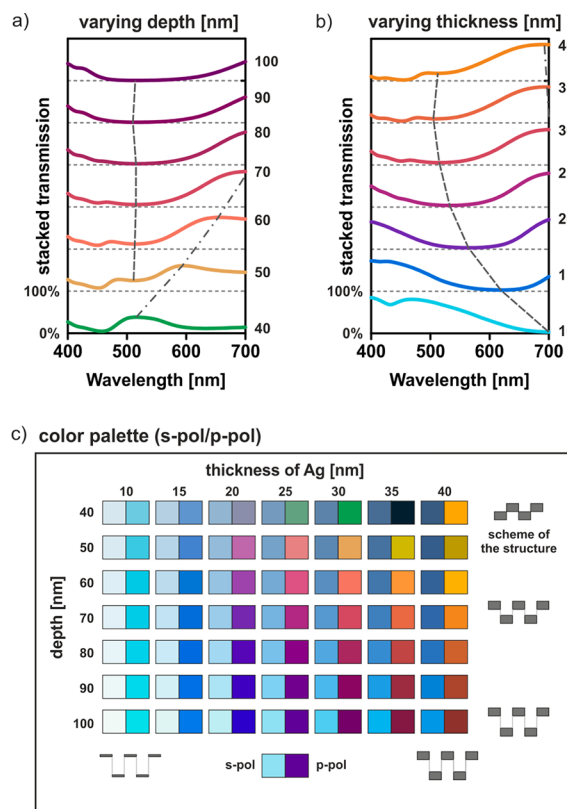
Figure 4. Calculated transmission spectra for p-polarized light and for (a) different periodic nanostructures depths (using 30 nm Ag) and (b) different silver thicknesses (using a depth of 70 nm). The LSPR (dashed) mainly depends on the thickness of the Ag, whereas a second mode (dot-dashed) is mainly influenced by the nanostructure depth. (c) Simulated color map of s-pol and p-pol colors for varying depth and silver thickness. The illustrations qualitatively indicate the arrangements. The spectra and color palette are colored in the computed transmission color.

(bold line), with 0° and 90° denoting s-pol and p-pol, respectively (Figure 5b). The intermediate colors (45° and 135°) show a very strong contrast. These appear in Figure 5a as purple/dark blue and orange/yellow. The colors span a wide range of the standard RGB color space (sRGB). A comparison between the images taken with and without analyzing polarizer is given in Figure S3. The photomask that we used to generate the image has five regions corresponding to different evaporation thicknesses (see Figure 5c). To further enhance the optical appearance, an analyzing polarizer was designed with two opposing regions (Figure 5c).

The color appearance depends mainly on two parameters: the spectra of the s-pol and p-pol states defining the basic colors (Figure 4c) and the spectral position of the LSPR, defining the intersection between the two intermediate spectra (Figure 1c). By appropriate choice of the nanowire geometry these parameters can be tuned to yield the ellipse in the CIE xyY color plot shown in Figure 5b. The size of the ellipse determines the contrast of the colors. For the geometry used in this report, the contrast is highest when the LSPR is located in the middle of the visible spectrum ($\lambda \sim 450-550$ nm). This was best fulfilled with using silver. Other materials are interesting as well and yield different basic colors. We also fabricated samples with gold and aluminum (data not shown) and varied the thicknesses of these nanowires. Using the measurement configuration of Figure 1c,

Figure 5. Color rendering and image formation. The measurement scheme of Figure 1c (diagonal input polarization) is used. (a) Images of Marilyn Monroe for four different analyzing polarizer settings (angle θ_2 is indicated). (b) Measured colors of Figure 1 are displayed in a CIE xyY color plot. The black triangle indicates the standard RGB color range. (c) Illustration of the mask consisting of five regions for different silver thicknesses (bold) and the analyzing polarizer. Derived from Original Artwork by Andy Warhol, The Andy Warhol Foundation for the Visual Arts, Inc., 2015, ProLitteris, Zurich.

we obtained four distinct colors, but often for the human eye, they do not show a strong contrast. Nevertheless, these materials are interesting to potentially increase the color palette, for example, green by using gold. Evaporation of different materials onto periodic nanostructures can lead to an optical color filter spanning the complete visible spectrum.

In this report we used silver nanowires and the configuration shown in Figure 1c for the following reasons. First, silver exhibits a pronounced resonance in the visible spectrum. Second, the geometry is simple, enabling large-scale fabrication and no implications for roll-to-roll manufacturing. Third, the fabricated structures are embedded, enabling use in ambient conditions. And fourth, a period of 160−180 nm shows a largely angle-independent behavior. Therefore, tilting the sample (up to ~60°) in any direction renders the same color appearance (see Figure S1), which is essential for usage in diffuse or poor light conditions. Consequently, this property of the proposed zero order effect clearly differs from analog diffractive grating effects.

In summary, we presented a 4-fold plasmonic color filter based on periodic silver nanowires. By rotation of an analyzing polarizer four distinct output colors and their intermediate states can be displayed. The wavelength-dependent transmission through the polarizer is a feature of the phase retardation of the plasmonic substrate. The underlying phase shift is induced by the plasmon resonance and results in high contrast colors. The palette of appearing colors can be enhanced by appropriate tuning of the fabrication process leading to geometrical variance of the nanowires. Angle- and orientation-stability of the transmitted color is granted by choosing an appropriate period of the nanowires enabling easy use even in diffuse light conditions. The complete fabrication process is integratable in a large-scale roll-to-roll process; the final device is designed such that it can be used at ambient conditions. Additionally, polarized light sources such as displays or smart phones can act as output polarizers enabling multiple and practical applications.

Extending our nanowire-based structures to 2D structures, permitting two plasmon resonances simultaneously, can further increase the contrast of the observed colors.[13,20] Aside from active color filtering, for example, for polarizing screens,[10] these structures could potentially be used as a valuable resource for

security applications,[15,37] magneto-optic (chromatic wave-plates),[38] polarizing detectors (e.g., polarization microscopy),[4] and sensing applications (e.g., refractive-index changes).[39]

■ METHODS

Fabrication. A periodic photoresist structure (4.7 cm × 4.7 cm) with a period of 160 nm and a duty cycle of 0.5 was obtained from e-beam lithography. Subsequently, a nickel shim was grown through a galvanic process to serve as a master structure. Replication was done in a UV curable polymer onto a glass substrate. After the curing process, 10−40 nm of silver was thermally evaporated onto the sample at 5×10^{-6} mbar and 3 Å/s. Subsequently, the structure was embedded with the UV curable polymer and a glass substrate.

Characterization. The transmission measurements were done with an Ocean Optics spectrometer (HR4000CG) with the sample fixed after a Glan-Thompson polarizer and the light source. A secondary polarizer was fixed on an automatic rotation stage for the transmission spectra (Figure 2). A PerkinElmer spectrometer (Lamba 9) was used to determine the transmission spectra of the different tilt angles. The size of the illumination spot was each about 3 × 3 mm, the measured samples were about 4.7 cm × 4.7 cm. The measured transmission values were transferred into RGB values with a homemade MATLAB script.

Computations. Near-field computations with the corresponding phase and charge density information were done with SIE.[32] First, far-field zero order transmission spectra were computed (300 nm to 900 nm, 0.5 nm step). The corresponding phase of the two polarized states and the difference could be evaluated directly. Second, near-field maps of the structure at the indicated wavelengths (see Figure 3c−e) were done (precision of 0.5 nm). The intensity is plotted logarithmically. Third, the charge density of the structure at the indicated wavelengths and at a given time was computed. Far-field computations were done with RCWA from 400 to 700 nm, in 0.5 nm steps for p-polarized light (see Figure 4). Computations were done for different depths of the structure (40−100 nm), different thicknesses of the silver (10−40 nm), different periods (not shown), and different materials (not shown).

Artwork Sample. An original artwork by Andy Warhol was used to create a simplified model of Marilyn Monroe. This served as a basis for several photomasks. Each outline depicted in Figure 5c shows a region with different silver thicknesses: ~15 nm (face), ~20 nm (background), ~26 nm (hair), ~30 nm (lips), and ~80 nm (black parts). Evaporation was done subsequently after exposure of the photoresist through the mask in a mask aligner. Finally, the substrate was embedded and an analyzing polarizer was designed as proposed in Figure 5c. The photographs were done with a SLR and by placing the sample onto the analyzing polarizer. Subsequent rotation of a polarizer led to the four distinct images.

■ ASSOCIATED CONTENT

Ⓢ Supporting Information
The Supporting Information is available free of charge on the ACS Publications website at DOI: 10.1021/acsphotonics.5b00604.

> Figure S1 shows a scheme of the measurement angles and transmission plots of the plasmonic structure. Figure S2 gives more details about the near-field effects around the plasmon resonance. A comparison of the color effect depending on the setup is given in Figure S3 (PDF).

■ AUTHOR INFORMATION

Corresponding Author
*E-mail: benjamin.gallinet@csem.ch. Tel.: +41616906028.

Notes
The authors declare no competing financial interest.

■ ACKNOWLEDGMENTS

■ ABBREVIATIONS

LSPR, localized surface plasmon resonance; PPR, plasmonic phase retarder; θ_1, angle of input polarizer; θ_2, angle of analyzing polarizer; s-pol, s-polarization; p-pol, p-polarization; φ_s, phase of s-pol; φ_p, phase of p-pol; φ_{diff} phase difference between s-pol and p-pol; *, λ_R, †, and #, positions before, at, above, and far above the plasmon resonance

■ REFERENCES

(1) Gu, Y.; Zhang, L.; Yang, J. K. W.; Yeo, S. P.; Qiu, C. Color Generation Via Subwavelength Plasmonic Nanostructures. *Nanoscale* **2015**, *7*, 6409−6419.

(2) Kumar, K.; Duan, H.; Hegde, R. S.; Koh, S. C. W.; Wei, J. N.; Yang, J. K. W. Printing Colour at the Optical Diffraction Limit. *Nat. Nanotechnol.* **2012**, *7*, 557−561.

(3) Zeng, B.; Gao, Y.; Bartoli, F. J. Ultrathin Nanostructured Metals for Highly Transmissive Plasmonic Subtractive Color Filters. *Sci. Rep.* **2013**, *3*, 1−9.

(4) Ellenbogen, T.; Seo, K.; Crozier, K. B. Chromatic Plasmonic Polarizers for Active Visible Color Filtering and Polarimetry. *Nano Lett.* **2012**, *12*, 1026−1031.

(5) Shrestha, V. R.; Lee, S.; Kim, E.; Choi, D. Aluminum Plasmonics Based Highly Transmissive Polarization-Independent Subtractive Color Filters Exploiting a Nanopatch Array. *Nano Lett.* **2014**, *14*, 1−7.

(6) Zeng, B.; Gao, Y.; Bartoli, F. J. Ultrathin Nanostructured Metals for Highly Transmissive Plasmonic Subtractive Color Filters. *Sci. Rep.* **2013**, *3*, 2840.

(7) Barnes, W. L.; Dereux, A.; Ebbesen, T. W. Surface Plasmon Subwavelength Optics. *Nature* **2003**, *424*, 824−830.

(8) Kaplan, A. F.; Xu, T.; Jay Guo, L. High Efficiency Resonance-Based Spectrum Filters with Tunable Transmission Bandwidth Fabricated Using Nanoimprint Lithography. *Appl. Phys. Lett.* **2011**, *99*, 143111−1−3.

(9) Shrestha, V. R.; Lee, S.; Kim, E.; Choi, D. Polarization-Tuned Dynamic Color Filters Incorporating a Dielectric-Loaded Aluminum Nanowire Array. *Sci. Rep.* **2015**, *5*, 12450.

(10) Zheng, B. Y.; Wang, Y.; Nordlander, P.; Halas, N. J. Color-Selective and CMOS-Compatible Photodetection Based on Aluminum Plasmonics. *Adv. Mater.* **2014**, *26*, 6318−6323.

(11) Vilas, J. L.; Sanchez-Brea, L. M.; Bernabeu, E. Optimal Achromatic Wave Retarders Using Two Birefrigent Wave Plates. *Appl. Opt.* **2013**, *52*, 1892−1896.

(12) Kang, G.; Tan, Q.; Wang, X.; Jin, G. Achromatic Phase Retarder Applied to MWIR & LWIR Dual-Band. *Opt. Express* **2010**, *18*, 1695−1703.

(13) Li, T.; Liu, H.; Wang, S.; Yin, X.; Wang, F.; Zhu, S.; Zhang, X. Manipulating Optical Rotation in Extraordinary Transmission by Hybrid Plasmonic Excitations. *Appl. Phys. Lett.* **2008**, *93*, 021110.

(14) Biagioni, P.; Savoini, M.; Huang, J.; Duò, L.; Finazzi, M.; Hecht, B. Near-Field Polarization Shaping by a Near-Resonant Plasmonic Cross Antenna. *Phys. Rev. B: Condens. Matter Mater. Phys.* **2009**, *80*, 1−4.

(15) Zheng, G.; Mühlenbernd, H.; Kenney, M.; Li, G.; Zentgraf, T.; Zhang, S. Metasurface Holograms Reaching 80% Efficiency. *Nat. Nanotechnol.* **2015**, *10*, 308−312.

(16) Zhao, Y.; Alù, A. Manipulating Light Polarization with Ultrathin Plasmonic Metasurfaces. *Phys. Rev. B: Condens. Matter Mater. Phys.* **2011**, *84*, 205428.

(17) Huang, L.; Chen, X.; Mühlenbernd, H.; Zhang, H.; Chen, S.; Bai, B.; Tan, Q.; Jin, G.; Cheah, K.; Qiu, C.; Li, J.; Zentgraf, T.; Zhang, S. Three-Dimensional Optical Holography Using a Plasmonic Metasurface. *Nat. Commun.* **2013**, *4*, 1−8.

(18) Huang, Y.; Chen, W. T.; Tsai, W.; Wu, P. C.; Wang, C.; Sun, G.; Tsai, D. P. Aluminum Plasmonic Multicolor Meta-Hologram. *Nano Lett.* **2015**, *15*, 3122−3127.

(19) Sambles, J. R.; Bradbery, G. W.; Yang, F. Optical Excitation of Surface Plasmons: an Introduction. *Contemp. Phys.* **1991**, *32*, 173−183.

(20) Goh, X. M.; Zheng, Y.; Tan, S. J.; Zhang, L.; Kumar, K.; Qiu, C.; Yang, J. K. W. Three-Dimensional Plasmonic Stereoscopic Prints in Full Colour. *Nat. Commun.* **2014**, *5*, 1−8.

(21) Park, C.; Yoon, Y.; Shrestha, V. R.; Park, C.; Lee, S.; Kim, E. Electrically Tunable Color Filter Based on a Polarization-Tailored Nano-Photonic Dichroic Resonator Featuring an Asymmetric Subwavelength Grating. *Opt. Express* **2013**, *21*, 28783.

(22) Lee, K. M.; Tondiglia, V. P.; McConney, M. E.; Natarajan, L. V.; Bunning, T. J.; White, T. J. Color-Tunable Mirrors Based on Electrically Regulated Bandwidth Broadening in Polymer-Stabilized Cholesteric Liquid Crystals. *ACS Photonics* **2014**, *1*, 1033−1041.

(23) Franklin, D.; Chen, Y.; Vazquez-Guardado, A.; Modak, S.; Boroumand, J.; Xu, D.; Wu, S.-T.; Chanda, D. Polarization-Independent Actively Tunable Colour Generation on Imprinted Plasmonic Surfaces. *Nat. Commun.* **2015**, *6*, 7337.

(24) Xu, Q.; Chen, L.; Wood, M. G.; Sun, P.; Reano, R. M.; Wood, M. G.; Reano, R. M. Electrically Tunable Optical Polarization Rotation on a Silicon Chip Using Berry'S Phase. *Nat. Commun.* **2014**, *5*, 5337.

(25) Xu, T.; Wu, Y.; Luo, X.; Guo, L. J. Plasmonic Nanoresonators for High-Resolution Colour Filtering and Spectral Imaging. *Nat. Commun.* **2010**, *1*, 59.

(26) Tan, S. J.; Zhang, L.; Di Zhu; Goh, X. M.; Wang, Y. M.; Kumar, K.; Qiu, C.; Yang, J. K. W. Plasmonic Color Palettes for Photorealistic Printing with Aluminum Nanostructures. *Nano Lett.* **2014**, *14*, 4023−4029.

(27) Clausen, J. S.; Højlund-Nielsen, E.; Christiansen, A. B.; Yazdi, S.; Grajower, M.; Taha, H.; Levy, U.; Kristensen, A.; Mortensen, N. A. Plasmonic Metasurfaces for Coloration of Plastic Consumer Products. *Nano Lett.* **2014**, *14*, 4499−4504.

(28) Huang, C.; Wang, Q.; Yin, X.; Zhang, Y.; Li, J.; Zhu, Y. Break Through The Limitation of Malus' Law with Plasmonic Polarizers. *Adv. Opt. Mater.* **2014**, *2*, 723−728.

(29) Sun, S.; Ye, Z.; Guo, L.; Sun, N. Wide-Incident-Angle Chromatic Polarized Transmission on Trilayer Silver/Dielectric Nanowire Gratings. *J. Opt. Soc. Am. B* **2014**, *31*, 1211.

(30) Wu, Y. R.; Hollowell, A. E.; Zhang, C.; Guo, L. J. Angle-Insensitive Structural Colours Based on Metallic Nanocavities and Coloured Pixels beyond the Diffraction Limit. *Sci. Rep.* **2013**, *3*, 1194.

(31) Savenkov, S. N. Jones and Mueller Matrices: Structure, Symmetry Relations and Information Content. In *Light Scattering Reviews 4*; Kokhanovsky, A. A., Ed.; Praxis Publishing, 2009; pp 71−119.

(32) Gallinet, B.; Kern, A. M.; Martin, O. J. F. Accurate and Versatile Modeling of Electromagnetic Scattering on Periodic Nanostructures with a Surface Integral Approach. *J. Opt. Soc. Am. A* **2010**, *27*, 2261−2271.

(33) McPeak, K. M.; Jayanti, S. V.; Kress, S. J. P.; Meyer, S.; Iotti, S.; Rossinelli, A.; Norris, D. J. Plasmonic Films Can Easily Be Better: Rules And Recipes. *ACS Photonics* **2015**, *2*, 326−333.

(34) Christ, A.; Martin, O. J. F.; Ekinci, Y.; Gippius, N. A.; Tikhodeev, S. G. Symmetry Breaking in a Plasmonic Metamaterial at Optical Wavelength. *Nano Lett.* **2008**, *8*, 2171−2175.

(35) Moharam, M. G.; Gaylord, T. K. Rigorous Coupled-Wave Analysis of Planar-Grating Diffraction. *J. Opt. Soc. Am.* **1981**, *71*, 811−818.

(36) Fairchild, M. D. *Color Appearance Models*; John Wiley & Sons, 2013; pp 1−409.

(37) Lochbihler, H. Polarizing and Angle-Sensitive Color Filter in Transmittance for Security Feature Applications. *Adv. Opt. Technol.* **2015**, *4*, 1−7.

(38) Liu, M.; Zhang, X. Nano-Optics: Plasmon-Boosted Magneto-Optics. *Nat. Photonics* **2013**, *7*, 429−430.

(39) Shen, Y.; Zhou, J.; Liu, T.; Tao, Y.; Jiang, R.; Liu, M.; Xiao, G.; Zhu, J.; Zhou, Z.; Wang, X.; Jin, C.; Wang, J. Plasmonic Gold Mushroom arrays with Refractive Index Sensing Figures of Merit Approaching the Theoretical Limit. *Nat. Commun.* **2013**, *4*, 2381.